Int J Ind Chem (2016) 7:93–101
DOI 10.1007/s40090-015-0069-1

RESEARCH

Preparation and characterization of $(Co,Mn)(Co,Mn)_2O_4$/MgO catalysts

Hayder Muneam[1] · Salih Hadi[1] · Mohanad Mousa Kareem[1] · S. David Jackson[2]

Received: 29 April 2015 / Accepted: 11 December 2015 / Published online: 22 January 2016
© The Author(s) 2016. This article is published with open access at Springerlink.com

Abstract A $(Co,Mn)(Co,Mn)_2O_4$/MgO catalyst was prepared by simple co-precipitation from an aqueous solution of the mixed metal salts using sodium carbonate. The calcination of the precipitate was characterized by TGA and XRD showing the generation of $(Co,Mn)(Co,Mn)_2O_4$/MgO by 773 K. The catalyst had a surface area of 45 m^2 g^{-1} in the fully calcined state (873 K) and was characterized by XRD and TGA. Characterization by TPR of the catalyst calcined at different temperatures revealed an annealing process that lowered the surface energy of the catalyst thereby inhibiting reduction. The calcined catalyst was active for the dehydrogenation of isopropanol to acetone and propene with the peak reaction temperature ~428 K and a second reaction zone around 613 K related to strongly bound alcohol. Lattice oxygen was reactive from 463 K converting adsorbed alcohol into carbon dioxide.

Keywords Mixed oxide spinel · Co-precipitation · Thermogravimetric analysis · Isopropanol dehydrogenation

Introduction

Spinels represent a wide range of compounds all having the same general formula, AB_2O_4, where A and B are divalent and trivalent metal cations that typically sit in tetrahedral and octahedral holes in the oxygen lattice, respectively. There are three classifications of the spinel structure, normal spinel $(A)^{tet}[B_2]^{oct}O_4$, inverse spinel $(B)^{tet}[A,B]^{oct}O_4$, and random spinel $(B_{0.6}A_{0.33})^{tet}[A_{0.6}B_{1.33}]^{oct}O_4$. The spinel structure can also crystallize in either a cubic or tetragonal form, with the tetragonal form being generated by a Jahn–Teller deformation of the octahedral. Spinels have a wide variety of uses, for example, they can be used, as catalysts for oxygen evolution reaction [1–3], reduction of nitrogen oxides, oxidation of CO, hydrocarbons [4], decomposition of NO and hydrogenation of CO [5], as thermistors and as infrared sensors [6].

The structure of the mixed metal spinel $(Co,Mn)(Co,Mn)_2O_4$ is similar to a mixture of $MnCo_2O_4$ and $CoMn_2O_4$ [7, 8]. Methods used in the ceramics industry to prepare this spinel starting from manganese and cobalt oxide precursors require heat treatment at high temperatures (≥1172 K) and need long treatment times [9]. From this type of preparation method the powders produced have large particle sizes and low surface areas. A method to produce higher surface area metal oxides involves the decomposition of precursors and subsequent heat treatment at low temperatures. Several precursors have been used for the preparation of the mixed metal spinel: acetates [10], carbonates [4, 11], citrates [4], hydroxycarbonates [12] and several more complex compounds [13–20] and gels [21, 22]. Decomposition and heat treatment are usually carried out in oxygen or air at temperatures below 873 K, however the heat treatment can last from 1 h to a few days. Preparations at temperatures ≤353 K have also been reported [23, 24]. The type of treatment can affect the structure and surfactants have been used to control morphology of generate nanomaterials [25].

Spinels also have a significant role in catalysis. A recent study by Li et al. [26] has shown the potential of $CoMn_2O_4$

✉ S. David Jackson
david.jackson@glasgow.ac.uk

[1] Chemistry Department, College of Science, Babylon University, P.O. Box 4, Hillah, Babylon, Iraq

[2] Centre for Catalysis Research, WestCHEM, School of Chemistry, University of Glasgow, Glasgow G12 8QQ, Scotland, UK

in electrocatalysis, while another study has shown their efficacy in polymer degredation [27]. To obtain optimal use of a material in catalysis it is usual to disperse it on a support, which can stabilize small particles of the active phase and give physical strength. There are two common catalyst preparation methodologies, impregnation and co-precipitation. However, to produce a compound with a specific stoichiometry, co-precipitation is the preferred route. Nevertheless supported cobalt–manganese oxide spinel has been prepared on graphene by an impregnation route [28] and used as a bifunctional catalyst.

In this paper we report on the preparation and characterization of a $(Co,Mn)(Co,Mn)_2O_4/MgO$ catalyst. The catalyst was prepared by co-precipitation of the cobalt, manganese and magnesium nitrates by sodium carbonate followed by calcination of the precipitate at temperatures greater than 673 K. The effect of the calcination temperature studied. We believe that this is the first such study. Characterization of this catalyst was done by using a range of techniques such as powder X-ray diffraction (PXRD), scanning electron microscopy (SEM), thermogravimetric analysis (TGA) and surface area determination (BET). Its efficacy as a catalyst was examined in dehydrogenation of isopropyl alcohol (IPA).

Experimental

The catalyst was prepared by co-precipitation. $Co(NO_3)_2{\cdot}6H_2O$ (0.0398 mol, Alfa Aesar), $(C_4H_6)MnO_4{\cdot}4H_2O$ (0.042 mol, Alfa Aesar), and $Mg(NO_3)_2{\cdot}6H_2O$ (0.099 mol, Fluka) were weighed and dissolved in deionized water. The solution was heated with stirring to 348 K, then 95 cm^3 Na_2CO_3 (1 M) added dropwise until the pH of the solution reached 10. The solution was then left stirring at 348 K for 2 h to complete the reaction. The precipitate was filtered and washed repeatedly with deionised water (1 L) before being dried at 373 K overnight. Samples of the dried powder were then calcined at different temperatures (673, 773, 873, 973 and 1073 K) in a Carbolite MTF furnace using a ramp rate of 10 K min^{-1}.

Powder X-ray diffraction (XRD) was used to determine the crystalline phase for the samples. The X-ray pattern was obtained using a Siemens D500 X-ray diffractometer with a Cu$K\alpha$ X-ray source (1.5418 Å). The working voltage and current for the X-rays was 40 kV and 40 mA, respectively. The scan range of 2θ was 5°–85° with a step size of 0.02° and counting time of 15 s per step.

The surface area and pore size for each catalyst was determined using a Micromeritics Gemini II 2375 Surface Area Analyser. Approximately 0.04–0.05 g of catalyst was weighed into a glass sample tube and degassed in a flow of N_2 overnight at 383 K before the measurement was carried out. The BET equation used to determine the surface area:

Thermogravimetric analysis (TGA) of the catalysts, calcined at different temperatures, was performed in a SDTQ600 series combined TGA/DSC instrument. In each case the sample was heated from room temperature to 1273 K under flowing (100 cm^3 min^{-1}) 5 % N_2/H_2 or 2 % O_2/Ar at 10 K min^{-1}.

Scanning electron microscopy and energy dispersive X-ray spectroscopy (SEM–EDX) was used to study the morphology and surface features of the catalyst. The images were taken for each samples by using a Philips XL30ESEM instrument. The samples were coated by using a polaron SC7640 auto high resolution sputter coater with gold/palladium under vacuum condition with flow argon gas, then transferred for analysis.

The isopropanol dehydrogenation study was performed in a flow micro-reactor at atmospheric pressure. Catalyst (0.25 g) that had been calcined at 873 K was loaded into the reactor and a flow of argon (30 cm^3 min^{-1}) established. The catalyst was heated to 473 K, 10 K min^{-1} and held for 30 min at 473 K before being allowed to cool to room temperature. This process was used to remove any adsorbed water present on the surface of the catalyst. The catalyst was saturated with isopropanol (IPA) by flowing the argon through a bubbler that contained the alcohol and hence over the catalyst. The up-take was monitored by mass spectrometry. Once the exit concentration of IPA matched that of the inlet, it was assumed that the catalyst was saturated and the flow was switched back to pure argon. The catalyst was then heated at 5 K min^{-1} from room temperature to 673 K and held for 30 min.

Results and discussion

Thermogravimetric analysis/differential scanning calorimetry (TGA/DSC) was used to determine the minimum temperature required to calcine the dried precursor from the change in mass and thermal properties in relation to temperature. Figure 1 shows the TGA results while Fig. 2 outlines the DSC results. Figure 1 shows the loss percentage of weight and derivative weight loss profile of the dried catalyst precursor (carbonate) under a 2 % O_2/Ar flow, from this profile it can be seen that the weight loss happens in three events at 499, 716 and 1152 K. The weight loss is 40 % of total weight of the catalyst during calcination. The loss at 499 K is endothermic and can be assigned to the loss of adsorbed water, the second weight loss (~22 %) at 716 K can be assigned tothe decomposition of a carbonate [28]. From the mass loss we assign this to magnesium carbonate to give $(Co,Mn)(Co,Mn)_2O_4/MgO$ (this is in keeping with the XRD patterns shown in Fig. 3).

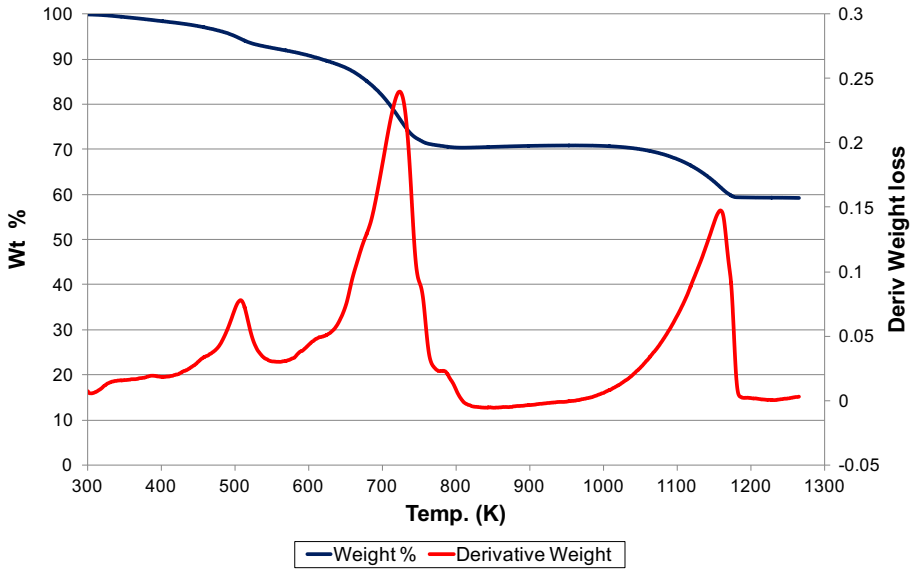

Fig. 1 TGA analysis of the as-prepared carbonate precursor under 2 % O_2/Ar

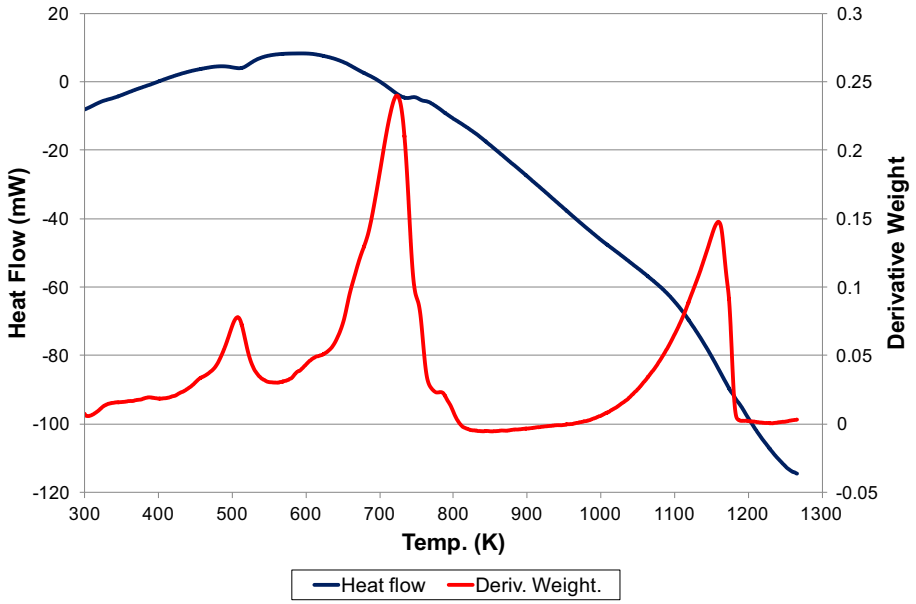

Fig. 2 DSC analysis of the as-prepared carbonate precursor under 2 % O_2/Ar

The high temperature weight loss (~10 %) at 1152 K can be assigned to the decomposition of the mixed oxide with the liberation of oxygen in a manner similar to that found with thermodynamically driven decomposition of Co_3O_4 spinel to CoO [29]. From these results a minimum calcination temperature of 673 K was chosen as at this temperature the carbonate precursor decomposes to the cobalt manganese oxide and magnesium oxide.

Powder X-ray diffraction (XRD) patterns of the material calcined at different temperatures are shown in Fig. 3. It is clear that the sample has, after calcination, converted to $(Co,Mn)(Co,Mn)_2O_4$/MgO in a manner reminiscent of the $Cu/ZnO/Al_2O_3$ methanol synthesis catalyst [30] where the calcination of the malachite precursor gives rise to $CuO/ZnO/Al_2O_3$. The presence of $(Co,Mn)(Co,Mn)_2O_4$ was confirmed by comparing the data with JPDS card no. 00-018-0408(N) and the presence of MgO was confirmed with JPDS card no. 00-003-0998(D). The MgO (111) reflection at ~37 2θ has not been assigned for clarity. There is some evidence in the XRD pattern for low levels of tetragonal $CoMn_2O_4$ [31].

Analysis of XRD profile using the Scherrer equation allowed the determination of particle sizes for both $(Co,Mn)(Co,Mn)_2O_4$ and MgO. The (311) reflection at ~36 2θ was used for the $(Co,Mn)(Co,Mn)_2O_4$, while the (200) reflection at ~42 2θ was used for the MgO. The results are tabulated in Table 1. As expected as the temperature of calcination increases the particle size increases.

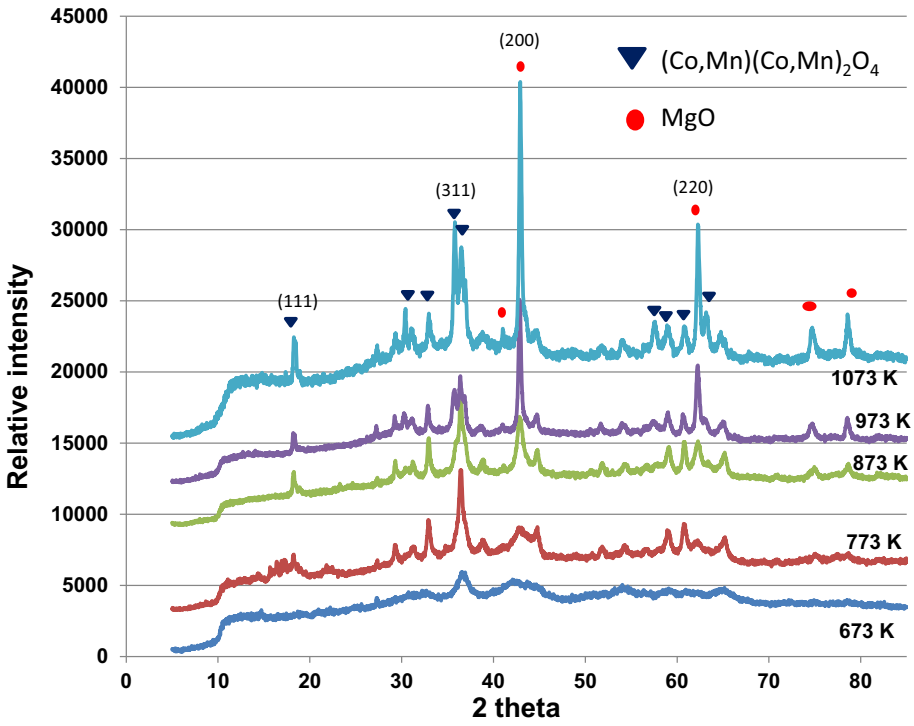

Fig. 3 XRD patterns of $(Co,Mn)(Co,Mn)_2O_4$/MgO at different calcination temperatures

Crystallites of $(Co,Mn)(Co,Mn)_2O_4$ in this size range have been shown in a recent XPS study [32] to have mixed valency cobalt and manganese ions with Co^{2+}, Co^{3+}, Co^{4+}, Mn^{2+}, Mn^{3+} and Mn^{4+} all present. As the particle size decreased the amounts of Co^{3+}, Co^{4+} and Mn^{4+} increased as well as Mn^{2+} to maintain charge balance. Magnetic studies of $CoMn_2O_4$ nanoparticles [33] of a size similar to that produced here revealed that the ferrimagnetic ordering, the coercivity and the remnant field are dependent on the particle size.

SEM images shown in Fig. 4, reveal the morphology of the catalyst at each calcination temperature. At low calcination temperatures, the SEM images of the catalyst show a separate border between particles of catalyst, this border disappears gradually with increasing calcination temperature. The SEM–EDX spectra (Fig. 5) was used for elemental analysis and confirmed that only peaks that corresponding to Co, Mn, Mg and O were present.

Table 1 Effect of temperature on the $(Co,Mn)(Co,Mn)_2O_4$/MgO sample particle size

	Temperature (K)			
	773	873	973	1073
$(Co,Mn)(Co,Mn)_2O_4$	5.3 nm	5.5 nm	6.3 nm	17.1 nm
MgO	NM	2.3 nm	19.4 nm	27.1 nm

NM not measured

Table 2 shows the surface areas, pore volumes and pore diameters of the catalyst after calcination at different temperatures. It can be seen that the surface area decreases with increasing calcination temperature due to sintering at high temperatures [29, 34–36]. This is in agreement with the hot stage XRD, which showed an increase in particle size.

To further investigate the effect of the calcination process the catalysts were subjected to a temperature programmed reduction after calcination. Figures 6 and 7 show the TGA plots for the catalysts while being subjected to a H_2/N_2 flow. It is clear that as the calcination temperature increases the weight loss under hydrogen/nitrogen decreases (Fig. 8).

The weight loss at ~363 K can be assigned to the loss of adsorbed water. It is noticeable that as the calcination temperature increases the amount of this water decreases. This is due to annealing of the surface structure and removal of any surface hydroxyl groups. As the number of surface hydroxyls is reduced so the ability of the crystal to adsorb water is reduced. The higher temperature weight losses are indicative of reduction of the cobalt manganese oxide. The sample calcined at 673 K loses ~25 % of its weight which is equivalent to full reduction of the $(Co,Mn)(Co,Mn)_2O_4$/MgO to give a Co-Mn/MgO material, i.e. both the cobalt and the manganese have been reduced to metal. The main reduction events are around 615 K and show a complex pattern as would be expected with the range of reducible species present. As the calcination

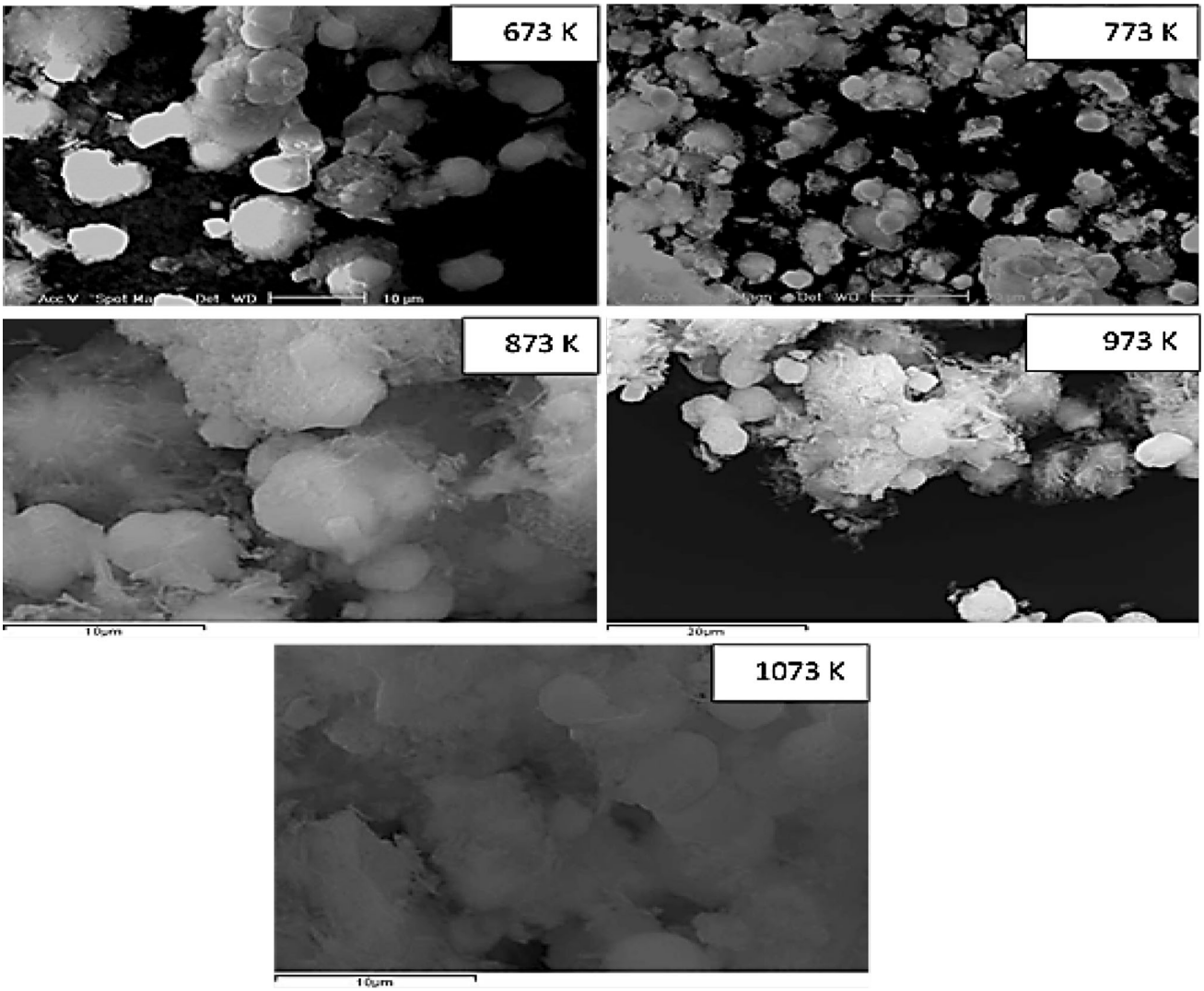

Fig. 4 SEM images of $(Co,Mn)(Co,Mn)_2O_4/MgO$. All images have the same magnification of $\times 1000$

Fig. 5 SEM–EDX spectrum of calcined catalyst

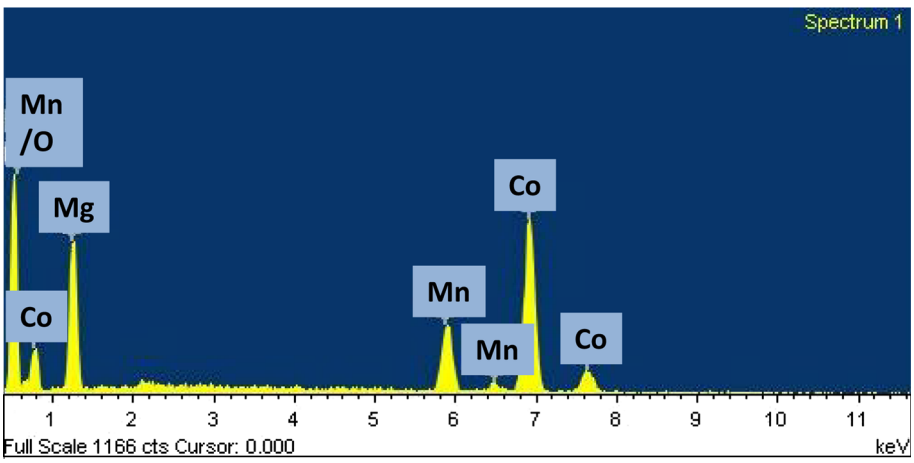

Table 2 BET surface areas of sample after heating to different temperatures

Temp. of calcination (K)	Surface area (m^2 g^{-1})	Average pore volume (cm^3 g^{-1})	Average pore diameter (nm)
673	71	0.22	12.3
773	50	0.26	20.7
873	45	0.23	20.3
973	22	0.11	20.2
1073	9	0.02	8.1

temperature increases the amount of oxygen reduces such that after calcination at 873 K only half of the oxygen is removed (equivalent to two oxygen atoms) in two events at 600 and 728 K. This would in principle reduce all cobalt and manganese ions to Co^{2+} and Mn^{2+} ($CoMnO_2$). After calcination at 1073 K only the equivalent of one oxygen atom is removed from the $CoMn_2O_4$ in a single reduction event at 825 K. These results are in good agreement with the literature [37], where a single high temperature reduction peak was identified. The reduction was assigned to the reduction of Co^{2+} in a spinel environment, which

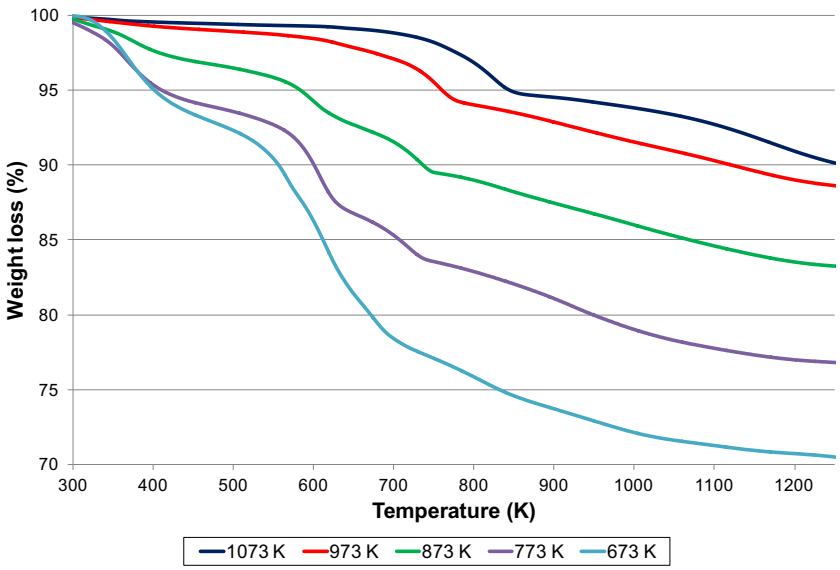

Fig. 6 TGA profiles under 2 % hydrogen/nitrogen for catalyst calcined at different temperatures

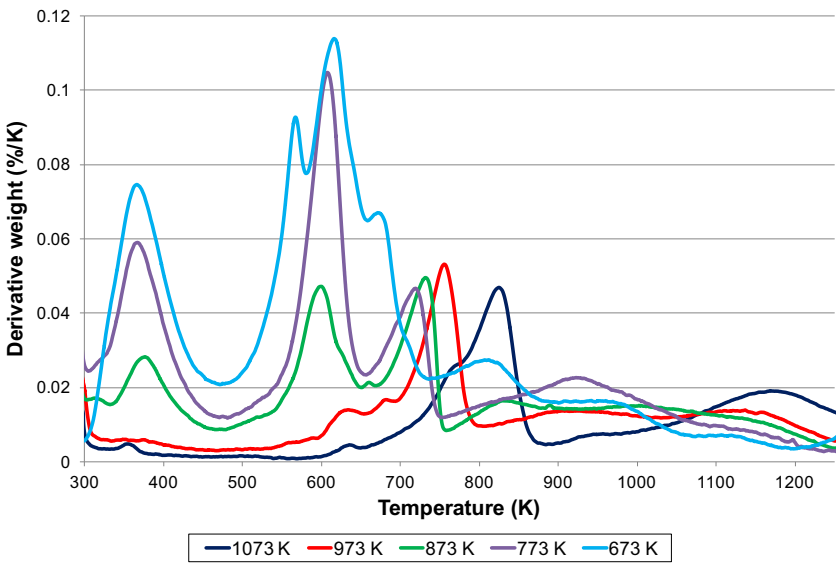

Fig. 7 Derivative weight profiles for reduction of $(Co,Mn)(Co,Mn)_2O_4/MgO$ after calcination at different temperatures

would agree with the loss of one oxygen atom from the complex. Therefore as the calcination temperature is increased the sample sinters (Table 1) and the surface area reduces (Table 2). These processes remove surface defects, including surface hydroxyls, decreasing the surface energy of the crystallites making it harder for reduction to occur.

The catalyst that had been calcined to 873 K, so ensuring that it was (Co,Mn)$(Co,Mn)_2O_4$/MgO, was tested for isopropanol dehydrogenation as outlined in the experimental section. The catalyst was saturated with IPA at room temperature then heated to 673 K. The temperature programmed desorption/reaction (TPDR) was followed by mass spectrometry and is shown in Fig. 9. IPA may react in two ways, to form propene by dehydration or to form acetone by dehydrogenation. The dehydration reaction has been shown to be diagnostic of acid sites, while the dehydrogenation is diagnostic for redox or basic sites [38]. In this reaction both products were detected.

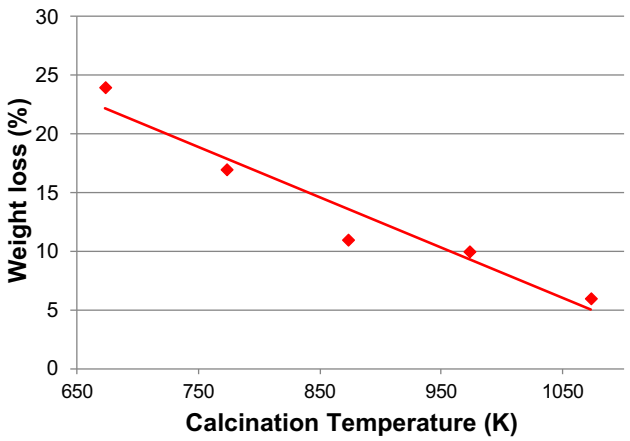

Fig. 8 Total weight loss from hydrogen reduction as a function of calcination temperature

The shape of the desorption peak of isopropanol and the reaction peak for acetone and propene are unusually shaped. The cause of this is the endothermic nature of the reactions. As they proceed heat is withdrawn faster than the furnace can replace it and the temperature of the catalyst bed falls before the furnace can adequately respond. Note that the vast majority of the isopropanol is reacted (the scale on the graph is two orders of magnitude larger for acetone and propene). Nevertheless the behavior of the reaction can be followed. Initially there is desorption of isopropanol and the peak desorption occurs 10 K below the peak reaction temperature of 428 K. Both propene and acetone are produced simultaneously. There is then a high temperature desorption/reaction around 613 K. Above 463 K carbon dioxide is also detected and this can be related to oxidation of the adsorbed isopropanol by the catalyst indicating that the lattice oxygen in the (Co,Mn)$(Co,Mn)_2O_4$ has been activated. This is in agreement with a study of IPA combustion over $CoMn_2O_4$ [37], where a Mars-van Krevelen mechanism was observed and the activity started just below 473 K.

Conclusions

A (Co,Mn)$(Co,Mn)_2O_4$/MgO catalyst was prepared by simple co-precipitation followed by calcination of the precipitate at temperatures greater than 673 K. The catalyst

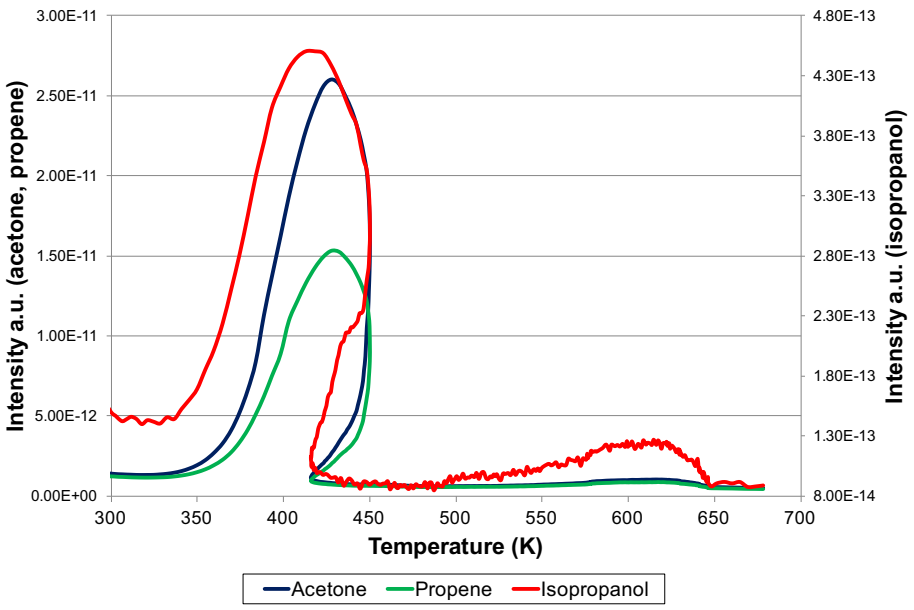

Fig. 9 Temperature programmed desorption/reaction of isopropanol

had a surface area of $\sim 70\ m^2\ g^{-1}$, which decreased to $9\ m^2\ g^{-1}$ as the calcination temperature was increased to 1073 K due to sintering of both the spinel and MgO phases. The catalyst was characterized by XRD and TGA. Both techniques confirmed the presence of $(Co,Mn)(Co,Mn)_2O_4$/MgO after calcination at temperatures above 673 K. Heating to temperatures above 1073 K resulted in the loss of oxygen from the spinel in a manner similar to that found with the high temperature transition between Co_3O_4 spinel and CoO. Characterization by TPR of the materials calcined at different temperatures revealed an annealing process that increased the particle size and lowered the surface energy of the catalyst thereby inhibiting reduction. With 673 K calcination it was possible to fully reduce the cobalt and manganese components, whereas after calcination at 1073 K the reduction was limited to the production of material with $CoMn_2O_3$ stoichiometry. The $(Co,Mn)(Co,Mn)_2O_4$/MgO catalyst was active for the dehydrogenation of isopropanol to acetone and propene with the peak reaction temperature ~ 428 K and a second reaction zone around 613 K related to strongly bound alcohol. Lattice oxygen was reactive from 463 K converting adsorbed alcohol into carbon dioxide. Therefore we have shown that using a straightforward preparation methodology an effective $CoMn_2O_4$/MgO catalyst, with a significant surface area, can be produced. The catalyst is active for acid/base and oxidation catalysis. The reduced form may be suitable for reaction such as Fischer–Tropsch or higher alcohol synthesis.

Authors' contributions HM, performed all experiments, processed data, initial data analysis and first draft of manuscript; MMK, guidance, SH, guidance, project design; SDJ, guidance, secondary data analysis, subsequent drafts of manuscript. All authors have read and approved the final manuscript.

Compliance with ethical standards

Conflict of interest The authors declare that they have no competing interests.

Open Access This article is distributed under the terms of the Creative Commons Attribution 4.0 International License (http://creativecommons.org/licenses/by/4.0/), which permits unrestricted use, distribution, and reproduction in any medium, provided you give appropriate credit to the original author(s) and the source, provide a link to the Creative Commons license, and indicate if changes were made.

References

1. Michio S, Masamichi O, Kenzo M (1997) Oxygen reduction catalysis of Mn–Co spinel oxides on a graphite electrode in alkaline solution. J Mater Chem 7:833–836
2. Rios E, Chartier P, Gautier J-L (1999) Oxygen evolution electrocatalysis in alkaline medium at thin $MnxCo_{3-x}O_4$ ($0 \leq x \leq 1$) spinel films on glass/SnO_2:F prepared by spray pyrolysis. Solid State Sci 1:267–277
3. Rios E, Poillerat G, Koenig JF, Gautier JL, Chartier P (1995) Preparation and characterization of thin Co_3O_4 and $MnCo_2O_4$ films prepared on glass/SnO_2:F by spray pyrolysis at 150 °C for the oxygen electrode. Thin Solid Films 264:18–24
4. Pirogova GN, Panich NM, Korosteleva RI, Voronin YuV, Popova NN (2000) Catalytic properties of chromites with a spinel structure in the oxidation of CO and hydrocarbons and reduction of nitrogen oxides. Russ Chem Bull 49:1536–2380
5. Qi L, Kaidong C, Wenhua H, Qijie Y (1998) CO hydrogenation over nanometer spinel-type Co/Mn complex oxides prepared by sol–gel method. Appl Catal 166:191–199
6. Nagatomo N, Endo K, Yonezawa T (1999) Infrared sensor using thin film ceramic semiconductor. Key Eng Mater 159–160:305–310
7. Zhenguo Y, Guanguang X, Simner PS, Stevenson JW (2005) Thermal growth and performance of manganese cobaltite spinel protection layers on ferritic stainless steel SOFC interconnects. J Electrochem Soc 152:A1896–A1901
8. Greenwood NN, Earnshaw A (1997) Chemistry of the elements. Butterworth Heinemann, Oxford, pp 247–249
9. Yingjia L, Jeffrey WF, Clarina DC (2013) Electrical properties, cation distributions, and thermal expansion of manganese cobalt chromite spinel oxides. J Am Ceram Soc 96:1841–1846
10. Dimitar G, Klissurski DG, Uzunova EL (2003) Cation-deficient nano-dimensional particle size cobalt–manganese spinel mixed oxides. Appl Surf Sci 214:370–374
11. Dyakova E, Terlecki BA, Mehandjiev D, Zhecheva E, Grbic B (1991) Oxidation of carbon monoxide over $Cu_{1-X}Cr_XCo_2O_4$ in the presence of sulfur oxides. React Kinet Catal Lett 43:521–526
12. Stoilova D, Koleva V (2000) IR study of solid phases formed in the $Mg(HCOO)_2$–$Cu(HCOO)_2$–H_2O system. J Mol Struct 553:131–139
13. Choi JP, Weil SK, Chou MY, Stevenson JW, Yang GZ (2011) Development of MnCoO coating with new aluminizing process for planar SOFC stacks. Int J Hydrogen Energy 36:4549–4556
14. Ravindranathan P, Mahesh GV, Patil KC (1987) Low-temperature preparation of fine-particle cobaltites. J Solid State Chem 66:20–25
15. Kui C, Fan Y, Guiling W, Jinling Y, Dianxue C (2013) Facile synthesis of porous $(Co, Mn)_3O_4$ nanowires free-standing on a Ni foam and their catalytic performance for H_2O_2 electroreduction. J Mater Chem A 1:1669–1676
16. Sivasankar BN, Govindarajan S (1996) hydrazine mixed metal malonates—new precursors for metal cobaltites. Mater Res Bull 31:47–54
17. Kun-Pyo H, Hee SP, Young-Uk K (1999) Trinuclear complexes $M[Co(en)_2(SO_3)_2]_2(H_2O)_2{\cdot}4H_2O$ (M = Mn, Fe, Co, Ni, Cu, Zn): their utilization for stoichiometric spinel oxides and the crystal structure of $Ni[Co(en)_2(SO_3)_2]_2(H_2O)_2{\cdot}4H_2O$. Bull Korean Chem Soc 20:163
18. de Vidales JLM, Vila E, Roja MR, Garcia-Martinez O (1995) Thermal behavior in air and reactivity in acid medium of cobalt manganese spinels $Mn_xCo_{3-x}O_4$ ($1 \leq x \leq 3$) synthesized at low temperature. Chem Mater 7:1716–1721
19. Tian YM, Yao Z, Sheng D, Mietek J, Shi Z (2014) Mesoporous $MnCo_2O_4$ with abundant oxygen vacancy defects as high-performance oxygen reduction catalysts. J Mater Chem A 2:8676
20. Salavati-Niasari M, Khansari A, Davar F (2009) Synthesis and characterization of cobalt oxide nanoparticles by thermal treatment process. Inorg Chim Acta 362:4937–4942
21. Youichi S, Masayuki S (2002) Optoelectrochemical hydrogen–phosphate ion sensor based on electrochromism of spinel-type oxide thin-film electrode. J Appl Phys 41:6243–6246
22. Rosa MR, Eladio V, Oscar G, José LMDV (1994) Thermal behaviour and reactivity of manganese cobaltites

$Mn_xCo_{3-x}O_4(0.0 \leq x \leq 1.0)$ obtained at low temperature. J Mater Chem 4:1635–1639
23. Yamamoto N, Higashi S, Kawano S, Achiwa N (1983) Preparation of $MnCo_2O_4$ by a wet method and its metal ion distribution. J Mater Sci Lett 2:525–526
24. Young I, Haifeng W, Yet MC (1998) Room-temperature synthesis of monodisperse mixed spinel $(Co_xMn_{1-x})_3O_4$ powder by a coprecipitation method. J Mater Chem 8:2761–2764
25. Salavati-Niasari M, Mir N, Davar F (2009) Synthesis and characterization of Co_3O_4 nanorods by thermal decomposition of cobalt oxalate. J Phys Chem Solids 70:847–852
26. Li C, Han X, Cheng F, Hu Y, Chen C, Chen J (2015) Phase and composition controllable synthesis of cobalt manganese spinel nanoparticles towards efficient oxygen electrocatalysis. Nat Commun 6:7345
27. Imran M, Kim DH, Al-Masry WA, Mahmood A, Hassan A, Haider S, Ramay SM (2013) Manganese-, cobalt-, and zinc-based mixed-oxide spinels as novel catalysts for the chemical recycling of poly(ethylene terephthalate) via glycolysis. Polym Degrad Stab 98:904–915
28. Wang L, Zhao X, Lu Y, Xu M, Zhang D, Ruoff RS, Stevenson KJ, Goodenough JB (2011) $CoMn_2O_4$ spinel nanoparticles grown on graphene as bifunctional catalyst for lithium-air batteries. J Electrochem Soc 158:A1379–A1382
29. Jing X, Song S, Wang J, Ge L, Jamil S, Liu Q, Mann T, He Y, Zhang M, Wei H, Liu L (2012) Solvothermal synthesis of morphology controllable $CoCO_3$ and their conversion to Co_3O_4 for catalytic application. Powder Technol 217:624–628
30. Spencer MS (1999) The role of zinc oxide in Cu/ZnO catalysts for methanol synthesis and the water–gas shift reaction. Top Catal 8:259–266
31. Ge X, Liu Y, Goh FWT, Hor TSA, Zong Y, Xiao P, Zhang Z, Lim SH, Li B, Wang X, Liu Z (2014) Dual-phase spinel $MnCo_2O_4$ and spinel $MnCo_2O_4$/nanocarbon hybrids for electrocatalytic oxygen reduction and evolution. ACS Appl Mater Interfaces 6:12684–12691
32. Zhang HT, Chen XH (2006) Size-dependent X-ray photoelectron spectroscopy and complex magnetic properties of $CoMn_2O_4$ spinel nanocrystals. Nanotechnology 17:1384–1390
33. Mahata P, Sarma D, Madhu C, Sundaresen A, Natarajan S (2011) $CoMn_2O_4$ spinel from a MOF: synthesis, structure and magnetic studies. Dalton Trans 40:1952–1960
34. Trasatti S (1990) Surface chemistry of oxides and electrocatalysis. Croat Chem Acta 63:313
35. Guiling W, Dianxue C, Cuilei Y, Yinyi G, Jinling Y, Lin C (2009) Nickel foam supported-Co_3O_4 nanowire arrays for H_2O_2 electroreduction. Chem Mater 21:5112–5118
36. Xun L, Changjin T, Man A, Lin D, Zheng X (2010) Controllable synthesis of pure-phase rare-earth orthoferrites hollow spheres with a Porous shell and their catalytic performance for the CO + NO reaction. Chem Mater 22:4879–4889
37. Hosseini SA, Salari D, Niaei A, Deganello F, Pantaleo G, Hojati P (2011) Chemical–physical properties of spinel $CoMn_2O_4$ nanopowders and catalytic activity in the 2-propanol and toluene combustion: Effect of the preparation method. J Environ Sci Health A 46:291–297
38. Aramendıa MA, Borau V, Jimenez C, Marinas JM, Porras A, Urbano FJ (1996) magnesium oxides as basic catalysts for organic processes study of the dehydrogenation–dehydration of 2-propanol. J Catal 161:829–838